Chapter 13

Forces in Confined Fields

As early as 1619 Johannes Kepler suggested that the mechanical effect of light might be responsible for the deflection of the tail of comets entering our solar system. The classical Maxwell theory showed in 1873 that the radiation field carries with it momentum and that "light pressure" is exerted on illuminated objects. In 1905 Einstein introduced the concept of the photon and showed that energy transfer between light and matter occurs in discrete quanta. Momentum and energy conservation was found to be of great importance in microscopic events. The discrete momentum transfer between photons (X-rays) and other particles (electrons) has been experimentally demonstrated by Compton in 1925 and the recoil momentum transferred from photons on atoms has been observed by Frisch in 1933 [1]. Important studies on the action of photons on neutral atoms were made in the 1970's by Letokhov and other researchers in the former USSR and in the group of Ashkin at the Bell Laboratories, USA. The latter group proposed bending and focusing of atomic beams and trapping of atoms in focused laser beams. Later work by Ashkin and co-workers led to the development of "optical tweezers". These devices allow to optically trap and manipulate macroscopic particles and living cells with typical sizes in the range of $0.1 - 10$ micrometers [2, 3]. Milliwatts of laser power produce piconewtons of force. Due to the high field gradients of evanescent waves, strong forces are to be expected in optical near-fields.

The idea that an object might cool through its interaction with the radiation field was suggested already in 1929 by Pringsheim [4]. However, the first proposal to cool atoms in counter-propagating laser beams was made by Hänsch and Schawlow in 1975 [5]. This proposal was the starting point for a series of exciting experiments which led to the 1997 Nobel prize in physics. The mechanical force in laser trapping and cooling experiments can be understood on a semiclassical basis where the electromagnetic field is treated classically and the particle being trapped as a quantized two-level system [6]. However, the quantum theory of photons is used for the correct

interpretation of the results [7]. Furthermore, the photon concept asserts that there are quanta of energy and momentum transfer between the radiation field and the atom.

In this chapter we use classical electrodynamics to derive the conservation law for linear momentum in an optical field. The net force exerted on an arbitrary object is entirely determined by Maxwell's stress tensor. In the limiting case of an infinitely extended object, the formalism renders the known formulas for radiation pressure. Similarly, in the small object limit, we obtain the familiar expressions for gradient and scattering forces. Using the expression for the atomic polarizability derived in Appendix **??** it is possible to derive the forces acting on atoms and molecules in optical traps. The theory is also applied to calculate the trapping forces near a laser illuminated metal tip.

13.1 Maxwell's stress tensor

The general law for forces in electromagnetic fields is based on the conservation law for linear momentum. We therefore derive this conservation law in the following. Later we will discuss two different limits, the dipolar limit and the limit of the planar interface. For simplicity, we consider Maxwell's equations in vacuum. In this case we have $\mathbf{D} = \varepsilon_o \mathbf{E}$ and $\mathbf{B} = \mu_o \mathbf{H}$. Later we will relax this constraint. The conservation law for linear momentum is entirely a consequence of Maxwell's equations

$$\nabla \times \mathbf{E}(\mathbf{r},t) = -\frac{\partial \mathbf{B}(\mathbf{r},t)}{\partial t} , \tag{13.1}$$

$$\nabla \times \mathbf{B}(\mathbf{r},t) = \frac{1}{c^2}\frac{\partial \mathbf{E}(\mathbf{r},t)}{\partial t} + \mu_o \mathbf{j}(\mathbf{r},t) , \tag{13.2}$$

$$\nabla \cdot \mathbf{E}(\mathbf{r},t) = \frac{1}{\varepsilon_o}\rho(\mathbf{r},t) , \tag{13.3}$$

$$\nabla \cdot \mathbf{B}(\mathbf{r},t) = \mathbf{0} , \tag{13.4}$$

and of the force law

$$\begin{aligned} \mathbf{F}(\mathbf{r},t) &= q\left[\mathbf{E}(\mathbf{r},t) + \mathbf{v}(\mathbf{r},t) \times \mathbf{B}(\mathbf{r},t)\right] \\ &= \int_V \left[\rho(\mathbf{r},t)\mathbf{E}(\mathbf{r},t) + \mathbf{j}(\mathbf{r},t) \times \mathbf{B}(\mathbf{r},t)\right] dV . \end{aligned} \tag{13.5}$$

The first expression applies to a single charge q moving with velocity $\mathbf{v}$ and the second expression to a distribution of charges and currents satisfying the charge conservation law

$$\nabla \cdot \mathbf{j}(\mathbf{r},t) + \frac{\partial \rho(\mathbf{r},t)}{\partial t} = 0 , \tag{13.6}$$

which is a direct consequence of Maxwell's equations. The force law connects the electromagnetic world with the mechanical one. The two terms in the first expression are basically definitions of the electric and magnetic field.

If we operate on Maxwell's first equation by $\times\varepsilon_o\mathbf{E}$, on the second equation by $\times\mu_o\mathbf{H}$, and then add the two resulting equations we obtain

$$\varepsilon_o(\nabla\times\mathbf{E})\times\mathbf{E}+\mu_o(\nabla\times\mathbf{H})\times\mathbf{H} \;=\; \mathbf{j}\times\mathbf{B}-\frac{1}{c^2}[\frac{\partial\mathbf{H}}{\partial t}\times\mathbf{E}]+\frac{1}{c^2}[\frac{\partial\mathbf{E}}{\partial t}\times\mathbf{H}]\,. \qquad (13.7)$$

We have omitted the arguments $(\mathbf{r},t)$ for the different fields and we used $\varepsilon_o\mu_o=1/c^2$. The last two expressions in Eq. (13.7) can be combined to $(1/c^2)\,d/dt\;[\mathbf{E}\times\mathbf{H}]$. For the first expression in Eq. (13.7) we can write

$$\varepsilon_o(\nabla\times\mathbf{E})\times\mathbf{E} \;= \qquad (13.8)$$

$$\varepsilon_o\begin{bmatrix}\partial/\partial x(E_x^2-E^2/2) & +\partial/\partial y(E_xE_y) & +\partial/\partial z(E_xE_z)\\ \partial/\partial x(E_xE_y) & +\partial/\partial y(E_y^2-E^2/2) & +\partial/\partial z(E_yE_z)\\ \partial/\partial x(E_xE_z) & +\partial/\partial y(E_yE_z) & +\partial/\partial z(E_z^2-E^2/2)\end{bmatrix}-\varepsilon_o\,\mathbf{E}\,\nabla\cdot\mathbf{E}$$

$$=\;\nabla\cdot[\varepsilon_o\mathbf{E}\mathbf{E}\,-\,(\varepsilon_o/2)E^2\;\vec{\mathbf{I}}]-\rho\mathbf{E}\;.$$

where equation (13.3 has been used in the last step. The notation $\mathbf{EE}$ denotes the outer product, $E^2=E_x^2+E_y^2+E_z^2$ is the electric field strength, and $\vec{\mathbf{I}}$ denotes the unit tensor. A similar expression can be derived for $\mu_o(\nabla\times\mathbf{H})\times\mathbf{H}$. Using these two expressions in Eq. (13.7) we obtain

$$\nabla\cdot[\varepsilon_o\mathbf{E}\mathbf{E}\,-\,\mu_o\mathbf{H}\mathbf{H}\,-\,\frac{1}{2}\,(\varepsilon_oE^2+\mu_oH^2)\;\vec{\mathbf{I}}] \;=\; \frac{d}{dt}\frac{1}{c^2}[\mathbf{E}\times\mathbf{H}]+\rho\,\mathbf{E}\;+\;\mathbf{j}\times\mathbf{B}\;. \qquad (13.9)$$

The expression in brackets on the left hand side is called Maxwell's stress tensor in vacuum, usually denoted as $\vec{\mathbf{T}}$. In cartesian components it reads as

$$\vec{\mathbf{T}}=\;[\varepsilon_o\mathbf{E}\mathbf{E}-\mu_o\mathbf{H}\mathbf{H}\,-\,\frac{1}{2}\,(\varepsilon_oE^2+\mu_oH^2)\;\vec{\mathbf{I}}] \;= \qquad (13.10)$$

$$\begin{bmatrix}\varepsilon_o(E_x^2-E^2/2)\,+\,\mu_o(H_x^2-H^2/2) & \varepsilon_oE_xE_y\,+\,\mu_oH_xH_y & \varepsilon_oE_xE_z\,+\,\mu_oH_xH_z\\ \varepsilon_oE_xE_y\,+\,\mu_oH_xH_y & \varepsilon_o(E_y^2-E^2/2)\,+\,\mu_o(H_y^2-H^2/2) & \varepsilon_oE_yE_z\,+\,\mu_oH_yH_z\\ \varepsilon_oE_xE_z\,+\,\mu_oH_xH_z & \varepsilon_oE_yE_z\,+\,\mu_oH_yH_z & \varepsilon_o(E_z^2-E^2/2)\,+\,\mu_o(H_z^2-H^2/2)\end{bmatrix}.$$

After integration of Eq. (13.9) over an arbitrary volume V which contains all sources ρ and $\mathbf{j}$ we obtain

$$\int_V\nabla\cdot\vec{\mathbf{T}}\;dV \;=\; \frac{d}{dt}\frac{1}{c^2}\int_V[\mathbf{E}\times\mathbf{H}]\,dV\;+\;\int_V[\rho\,\mathbf{E}\;+\;\mathbf{j}\times\mathbf{B}]\,dV\;. \qquad (13.11)$$

The last term is recognized as the mechanical force [c.f. Eq. (13.5]. The volume integral on the left can be transformed to a surface integral using Gauss' integration law

$$\int_V \nabla\cdot \overleftrightarrow{\mathbf{T}}\; dV \;=\; \int_{\partial V} \overleftrightarrow{\mathbf{T}}\cdot\mathbf{n}\, da\;. \tag{13.12}$$

∂V denotes the surface of V, $\mathbf{n}$ the unit vector perpendicular to the surface, and da an infinitesimal surface element. We then finally arrive at the conservation law for linear momentum

$$\boxed{\int_{\partial V} \overleftrightarrow{\mathbf{T}}\,(\mathbf{r},t)\cdot\mathbf{n}(\mathbf{r})\, da \;=\; \frac{d}{dt}\left[\mathbf{G}_{field}\,+\,\mathbf{G}_{mech}\right]}\;. \tag{13.13}$$

Here, $\mathbf{G}_{mech}$ and $\mathbf{G}_{field}$ denote the mechanical momentum and the field momentum, respectively. In Eq. (13.13) we have used Newton's expression of the mechanical force $\mathbf{F} = d/dt\mathbf{G}_{mech}$ and the definition of the field momentum

$$\mathbf{G}_{field} \;=\; \frac{1}{c^2}\int_V [\mathbf{E}\times\mathbf{H}]\, dV\;. \tag{13.14}$$

This is the momentum carried by the electromagnetic field within the volume V. It is created by the dynamic terms in Maxwell's curl equations, i.e. by the terms containing the time derivative. The field momentum is zero when it is averaged over one oscillation period and the average force becomes

$$\boxed{\langle\mathbf{F}\rangle \;=\; \int_{\partial V} \langle\overleftrightarrow{\mathbf{T}}\,(\mathbf{r},t)\rangle\cdot\mathbf{n}(\mathbf{r})\; da}\;. \tag{13.15}$$

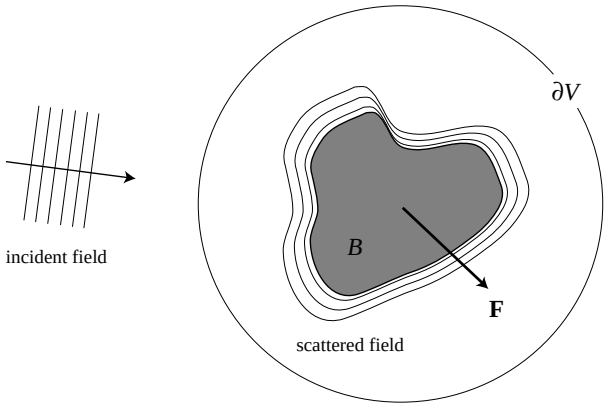

Figure 13.1: The mechanical force $\mathbf{F}$ acting on the object B is entirely determined by the electric and magnetic fields at an arbitrary surface ∂V enclosing B.

with $\langle .. \rangle$ denoting the time average. Equation (13.15(is of general validity. It allows to calculate the mechanical force acting on an arbitrary body within the closed surface ∂V. The force is entirely determined by the electric and magnetic fields on the surface ∂V. It is interesting to note that no material properties enter the expression for the force; the entire information is contained in the electromagnetic field. The only material constraint is that the body is rigid. If the body deforms when it is subject to an electromagnetic field we have to include electro- and magnetorestrictive forces. Since the enclosing surface is arbitrary the same results are obtained whether the fields are evaluated at the surface of the body or in the farfield. It is important to note that the fields used to calculate the force are the self-consistent fields of the problem which means that they are a superposition of the incident and the scattered fields. Therefore, prior to calculating the force, one has to solve for the electromagnetic fields. If the object B is surrounded by a medium which can accurately enough be represented by the dielectric constant ε and magnetic susceptibility μ the mechanical force can be calculated in the same way if we replace Maxwell's stress tensor Eq. (13.10) by

$$\boxed{\overleftrightarrow{\mathbf{T}} = [\varepsilon_o \varepsilon \mathbf{EE} - \mu_o \mu \mathbf{HH} - \frac{1}{2}(\varepsilon_o \varepsilon E^2 + \mu_o \mu H^2)\, \overleftrightarrow{\mathbf{I}}]} \,. \tag{13.16}$$

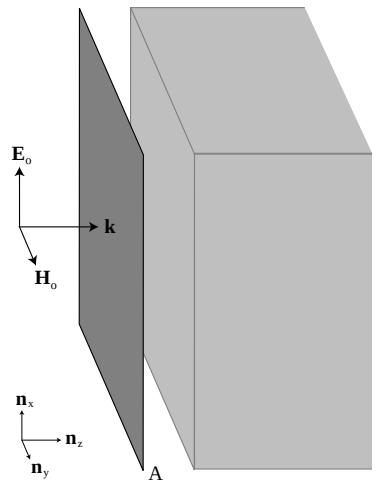

Figure 13.2: Configuration used to derive the radiation pressure.

13.2 Radiation pressure

Here, we consider the radiation pressure on a medium with an infinitely extended planar interface as shown in Fig. 13.2. The medium is irradiated by a monochromatic plane wave at normal incidence to the interface. Depending on the material properties of the medium, part of the incident field is reflected at the interface. Introducing the complex reflection coefficient R, the electric field outside the medium can be written as the superposition of two counter propagating plane waves

$$\mathbf{E}(\mathbf{r},t) \;=\; E_o\,\mathrm{Re}\Big\{\left[e^{ikz} \;+\; R\,e^{-ikz}\right]e^{-i\omega t}\Big\}\,\mathbf{n}_x\;. \tag{13.17}$$

Using Maxwell's curl equation (13.1 we find for the magnetic field

$$\mathbf{H}(\mathbf{r},t) \;=\; \sqrt{\varepsilon_o/\mu_o}\;E_o\,\mathrm{Re}\Big\{\left[e^{ikz} \;-\; R\,e^{-ikz}\right]e^{-i\omega t}\Big\}\,\mathbf{n}_y\;. \tag{13.18}$$

To calculate the radiation pressure P we integrate Maxwell's stress tensor on an infinite planar surface A parallel to the interface as shown in Fig. 13.2. The radiation pressure can be calculated by using Eq. (13.15) as

$$P\,\mathbf{n}_z \;=\; \frac{1}{A}\int_A \langle\overleftrightarrow{\mathbf{T}}\,(\mathbf{r},t)\rangle\cdot\mathbf{n}_z\;da\;. \tag{13.19}$$

We do not need to consider a closed surface ∂V since we are interested in the pressure exerted on the interface of the medium and not in the mechanical force acting on the medium. Using the fields of Eqs. (13.17) and (13.18) we find that the first two terms in Maxwell's stress tensor Eq. (13.10) give no contribution to the radiation pressure. The third term yields

$$\langle\overleftrightarrow{\mathbf{T}}\,(\mathbf{r},t)\rangle\cdot\mathbf{n}_z \;=\; -\frac{1}{2}\,\langle\varepsilon_o E^2+\mu_o H^2\rangle\,\mathbf{n}_z \;=\; \frac{\varepsilon_o}{2}\,E_o^2\,\left[1+|R|^2\right]\mathbf{n}_z\;. \tag{13.20}$$

Using the definition of the intensity of a plane wave $I_o \;=\; (\varepsilon_o/2)\,c\,E_o^2$, c being the vacuum speed of light, we can express the radiation pressure as

$$P \;=\; \frac{I_o}{c}\,\left[1\;+\;|R|^2\right]\,. \tag{13.21}$$

For a perfectly absorbing medium we have $R = 0$, whereas for a perfectly reflecting medium $R = 1$. Therefore, the radiation pressure on a perfectly reflecting medium is twice as high as for a perfectly absorbing medium.

13.3 The dipole approximation

A quantized two-level system such as an atom with transitions restricted to two states is well described by a dipole. The same is true for a macroscopic particle with

dimensions much smaller than the wavelength of the illuminating light (Rayleigh particle). To derive the electromagnetic force acting on a dipole we consider two oppositely charged particles with masses m_1, m_2, separated by a tiny distance $|\mathbf{s}|$, and illuminated by an arbitrary electromagnetic field $\mathbf{E}$, $\mathbf{B}$, as shown in Fig. 13.3. In the nonrelativistic limit, the equation of motion for each particle follows from Eq. (13.5) by setting $\mathbf{F}$ equal to $m_1\ddot{\mathbf{r}}_1$ and $m_2\ddot{\mathbf{r}}_2$, respectively. The dots denote differentiation with respect to time. Since the particles are bound to each other we have to consider their binding energy U. Including this contribution, the equation of motion for the two particles reads as

$$m_1\,\ddot{\mathbf{r}}_1 \;=\; q\,[\mathbf{E}(\mathbf{r}_1,t) \,+\, \dot{\mathbf{r}}_1\times\mathbf{B}(\mathbf{r}_1,t)] \,-\, \nabla U(\mathbf{r}_1,t)\,, \tag{13.22}$$

$$m_2\,\ddot{\mathbf{r}}_2 \;=\; -q\,[\mathbf{E}(\mathbf{r}_2,t) \,+\, \dot{\mathbf{r}}_2\times\mathbf{B}(\mathbf{r}_2,t)] \,+\, \nabla U(\mathbf{r}_2,t)\,. \tag{13.23}$$

The two particles constitute a two body problem which is most conveniently solved by introducing the center of mass coordinate

$$\mathbf{r} \;=\; \frac{m_1}{m_1+m_2}\,\mathbf{r}_1 \,+\, \frac{m_2}{m_1+m_2}\,\mathbf{r}_2\,. \tag{13.24}$$

Expressing the problem in terms of $\mathbf{r}$ allows us to separate the internal motion of the two particles from the center of mass motion. The electric field at the position of the two particles can be represented by a Taylor expansion as

$$\mathbf{E}(\mathbf{r}_1) \;=\; \sum_{n=0}^{\infty}\frac{1}{n!}\Big[(\mathbf{r}_1-\mathbf{r})\cdot\nabla\Big]^n\,\mathbf{E}(\mathbf{r}) \;=\; \mathbf{E}(\mathbf{r}) + (\mathbf{r}_1-\mathbf{r})\cdot\nabla\mathbf{E}(\mathbf{r}) \,+\, \ldots\,, \tag{13.25}$$

$$\mathbf{E}(\mathbf{r}_2) \;=\; \sum_{n=0}^{\infty}\frac{1}{n!}\Big[(\mathbf{r}-\mathbf{r}_2)\cdot\nabla\Big]^n\,\mathbf{E}(\mathbf{r}) \;=\; \mathbf{E}(\mathbf{r}) - (\mathbf{r}_2-\mathbf{r})\cdot\nabla\mathbf{E}(\mathbf{r}) \,+\, \ldots\,.$$

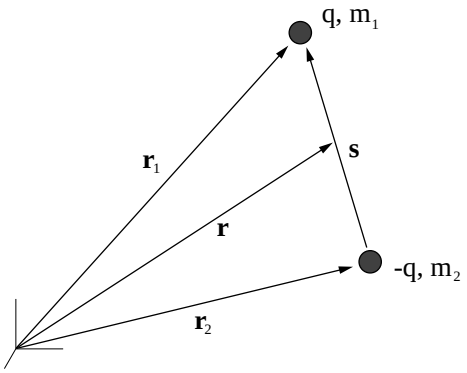

Figure 13.3: Graphical representation of the symbols used to derive the mechanical force in the dipolar limit. $\mathbf{r}$ denotes the center of mass coordinate. The two particles are bound to each other by the potential U.

A similar expansion can be found for $\mathbf{B}(\mathbf{r}_1)$ and $\mathbf{B}(\mathbf{r}_2)$. For $|\mathbf{s}| \ll \lambda$, λ being the wavelength of the radiation field, the expansions can be truncated after the second term (dipole approximation). A straight forward calculation using equations 13.22-13.25 and the definition of the dipole moment

$$\boldsymbol{\mu} \;=\; q\,\mathbf{s}\,, \tag{13.26}$$

where $\mathbf{s} = \mathbf{r}_1 - \mathbf{r}_2$ leads to the following formula for the total force $\mathbf{F} = (m_1+m_2)\ddot{\mathbf{r}}$ acting on the system of particles

$$\boxed{\mathbf{F} \;=\; (\boldsymbol{\mu}\cdot\nabla)\,\mathbf{E} \;+\; \dot{\boldsymbol{\mu}}\times\mathbf{B} \;+\; \dot{\mathbf{r}}\times(\boldsymbol{\mu}\cdot\nabla)\,\mathbf{B}}\;. \tag{13.27}$$

Here, we have omitted the arguments $(\mathbf{r}, t)$ for clarity. The brackets in $(\boldsymbol{\mu}\cdot\nabla)\,\mathbf{E}$ indicate that the inner product $\boldsymbol{\mu}\cdot\nabla = (\mu_x, \mu_y, \mu_z)\cdot(\partial/\partial x, \partial/\partial y, \partial/\partial z)$ has to be evaluated prior to operating on $\mathbf{E}$. Equation (13.27) is the central equation of this section. It renders the mechanical force exerted by the electromagnetic field on the two particles represented by the dipole moment $\boldsymbol{\mu}$. The force consists of three terms: the first originates from the inhomogeneous electric field, the second is the familiar Lorentz force, and the third is due to movement in the inhomogeneous magnetic field. Usually, the third term is much smaller than the other two terms and it will be omitted in the following discussion. It is interesting to note that the fields appearing in Eq. (13.27) correspond to the exciting field. It is assumed that the system represented by the dipole does not change the fields. This is different to the general formalism based on Maxwell's stress tensor where the self-consistent fields are considered.

13.3.1 Time-averaged force

The second term in Eq. (13.27) can be represented as

$$\dot{\boldsymbol{\mu}}\times\mathbf{B} \;=\; -\boldsymbol{\mu}\times\frac{d}{dt}\mathbf{B} \;+\; \frac{d}{dt}\,(\boldsymbol{\mu}\times\mathbf{B}) \;=\; \boldsymbol{\mu}\times(\nabla\times\mathbf{E}) \;+\; \frac{d}{dt}\,(\boldsymbol{\mu}\times\mathbf{B})\;. \tag{13.28}$$

We have approximated $d\mathbf{B}/dt$ by $\partial\mathbf{B}/\partial t$ because the velocity of the center of mass is assumed to be small compared with c. After dropping the last term in Eq. (13.27) for the same reason we obtain

$$\mathbf{F} \;=\; (\boldsymbol{\mu}\cdot\nabla)\,\mathbf{E} \;+\; \boldsymbol{\mu}\times(\nabla\times\mathbf{E}) \;+\; \frac{d}{dt}\,(\boldsymbol{\mu}\times\mathbf{B})\;, \tag{13.29}$$

which can be rewritten as

$$\mathbf{F} \;=\; \sum_i \mu_i \nabla E_i \;+\; \frac{d}{dt}\,(\boldsymbol{\mu}\times\mathbf{B})\;, \qquad i = x, y, z \tag{13.30}$$

In the time average, the last term vanishes, and the force can be cast into the concise form

$$\boxed{\langle \mathbf{F} \rangle \;=\; \sum_i \langle \mu_i(t)\, \nabla E_i(t) \rangle} \;, \tag{13.31}$$

where $\langle .. \rangle$ denotes the time-average. We have included the arguments of $\boldsymbol{\mu}$ and $\mathbf{E}$ in order to distinguish them from their corresponding complex amplitudes introduced below.

13.3.2 Monochromatic fields

Consider a dipolar particle irradiated by an arbitrary monochromatic electromagnetic wave with angular frequency ω. In this case the fields can be represented as*

$$\begin{aligned} \mathbf{E}(\mathbf{r},t) &= \mathrm{Re}\{\underline{\mathbf{E}}(\mathbf{r})\, e^{-i\omega t}\} \\ \mathbf{B}(\mathbf{r},t) &= \mathrm{Re}\{\underline{\mathbf{B}}(\mathbf{r})\, e^{-i\omega t}\}\;. \end{aligned} \tag{13.32}$$

If there is a linear relationship between dipole and fields, the dipole assumes the same time-dependence and can be written as

$$\boldsymbol{\mu}(t) \;=\; \mathrm{Re}\{\underline{\boldsymbol{\mu}}\, e^{-i\omega t}\}\;. \tag{13.33}$$

We assume that the particle has no static dipole moment. In this case, to first order, the induced dipole moment is proportional to the electric field at the particle's position $\mathbf{r}$

$$\underline{\boldsymbol{\mu}} \;=\; \alpha(\omega)\, \underline{\mathbf{E}}(\mathbf{r}_o)\;, \tag{13.34}$$

where α denotes the polarizability of the particle. Its form depends on the nature of the particle. For a two-level system, explicit expressions for α are derived in Appendix **??**. Generally, α is a tensor of rank two, but for atoms and molecules it is legitimate to use a scalar representation since only the projection of $\boldsymbol{\mu}$ along the direction of the electric field is important.

The cycle-average of Eq. (13.27) reads as

$$\langle \mathbf{F} \rangle \;=\; \frac{1}{2}\mathrm{Re}\left\{ (\underline{\boldsymbol{\mu}}^*\cdot\nabla)\, \underline{\mathbf{E}} \;-\; i\omega\, (\underline{\boldsymbol{\mu}}^*\times\underline{\mathbf{B}}) \right\}\;, \tag{13.35}$$

where we have dropped the third term as discussed before. The two terms on the right hand side can be combined as done before and we obtain

$$\langle \mathbf{F} \rangle \;=\; \sum_i \frac{1}{2}\mathrm{Re}\left\{ \underline{\mu}_i^*\, \nabla \underline{E}_i \right\} \;=\; \frac{1}{4}\nabla\left(\underline{\boldsymbol{\mu}}^*\cdot\underline{\grave{\mathbf{E}}} \;+\; \underline{\boldsymbol{\mu}}\cdot\underline{\grave{\mathbf{E}}}^* \right)\;, \tag{13.36}$$

*For clarity, we will designate the complex amplitudes of the fields by an underline.

where in the second expression ∇ acts *only* on the accented electric field $\underline{\grave{\mathbf{E}}}$. Using the linear relationship in Eq. (13.34) and representing the complex amplitude of the electric field in terms of the real amplitude E_o and phase ϕ as

$$\underline{\mathbf{E}}(\mathbf{r}) \;=\; E_o(\mathbf{r})\, \mathrm{e}^{i\phi(\mathbf{r})}\, \mathbf{n}_E \;, \tag{13.37}$$

with $\mathbf{n}_E$ denoting the unit vector in direction of the polarization, allows us to cast the cycle-averaged force into the following form

$$\boxed{\langle \mathbf{F} \rangle \;=\; \frac{\alpha'}{4} \nabla E_o^2 \;+\; \frac{\alpha''}{2} E_o^2 \nabla \phi} \;, \tag{13.38}$$

where we used $\alpha = \alpha' + i\alpha''$ and $\nabla E_o^2 = 2E_o \nabla E_o$. We find that two different terms determine the average mechanical force: the first is denoted as *dipole force* (or gradient force) and the second one as *scattering force*. The dipole force originates from field inhomogeneities. It is proportional to the dispersive part (real part) of the complex polarizability. On the other hand, the scattering force is proportional to the dissipative part (imaginary part) of the complex polarizability. The scattering force can be regarded as a consequence of momentum transfer from the radiation field to the particle. For a lossless particle there is no momentum transfer and the scattering force is zero. Polarizable particles are accelerated by the dipole force towards extrema of the radiation field. Therefore, a tightly focused laser beam can trap a particle in all dimensions at its focus. However, the scattering force pushes the particle in direction of propagation and if the focus of the trapping laser is not tight enough, the particle can be pushed out of the trap. Notice that ϕ can be written in terms of the local $\mathbf{k}$ vector as $\phi = \mathbf{k} \cdot \mathbf{r}$ which renders $\nabla\phi = \mathbf{k}$.

If we introduce Eq. (13.37) into Eq. (13.32), the time-dependent electric field can be written as

$$\mathbf{E}(\mathbf{r}, t) \;=\; E_o(\mathbf{r})\, \cos\left[\omega t - \phi(\mathbf{r})\right]\, \mathbf{n}_E \;. \tag{13.39}$$

The corresponding magnetic field is determined by $\partial \mathbf{B}/\partial t = -\nabla \times \mathbf{E}$ which, together with $\mathbf{E}$ leads to the relationships

$$E_o^2 \nabla \phi \;=\; 2\omega \langle \mathbf{E} \times \mathbf{B} \rangle \,, \quad E_o^2 \;=\; 2\langle |\mathbf{E}|^2 \rangle \,, \tag{13.40}$$

with $\langle .. \rangle$ denoting the cycle-average. Substituting into Eq. (13.38) gives

$$\boxed{\langle \mathbf{F} \rangle \;=\; \frac{\alpha'}{2} \nabla \langle |\mathbf{E}|^2 \rangle \;+\; \omega\, \alpha''\, \langle \mathbf{E} \times \mathbf{B} \rangle} \;, \tag{13.41}$$

where $|\mathbf{E}|$ denotes the time-dependent magnitude of the electric field vector. Eq. (13.41) directly proofs that the scattering force is proportional to the average field momentum defined in Eq. (13.14).

13.3.3 Saturation behavior for near-resonance excitation

Saturation is a nonlinear effect which limits the magnitude of the induced dipole moment $\boldsymbol{\mu}$. Different to most nonlinear effects, saturation does not affect the monochromatic time-dependence of the induced dipole (see Appendix **??**). Therefore, the linear relationship in Eq. (13.34) is valid even for saturation. The steady-state polarizability for a two-level atom excited near its resonance has been derived in Appendix **??**. Using the projection of the transition dipole moment along the direction of the electric field ($\boldsymbol{\mu}_{12}\cdot\mathbf{n}_E$) the polarizability can be written as

$$\alpha(\omega) \;=\; \frac{(\boldsymbol{\mu}_{12}\cdot\mathbf{n}_E)^2}{\hbar}\;\frac{(\omega_o-\omega+i\gamma/2)}{(\omega_o-\omega)^2+i\gamma^2/4+\omega_R^2/2}\,. \tag{13.42}$$

Here, ω_o is the transition frequency, $\omega_R=(\boldsymbol{\mu}_{12}\cdot\mathbf{n}_E)\,E_o/\hbar$ the Rabi frequency, and γ the spontaneous decay rate. Substituting α into Eq. (13.38) leads to

$$\langle\mathbf{F}\rangle \;=\; \hbar\frac{\omega_R^2/2}{(\omega_o-\omega)^2+i\gamma^2/4+\omega_R^2/2}\;\left[(\omega-\omega_o)\frac{\nabla E_o}{E_o}\;+\;\frac{\gamma}{2}\nabla\phi\right]\;. \tag{13.43}$$

Introducing the so-called *saturation parameter* p as

$$p \;=\; \frac{I}{I_{sat}}\,\frac{\gamma^2/4}{(\omega-\omega_o)^2+\gamma^2/4}\,, \tag{13.44}$$

with the intensity I and the saturation intensity I_{sat} defined as

$$I=\frac{\varepsilon_o c}{2}E_o^2\,,\quad I_{sat}=4\pi\varepsilon_o\frac{\hbar^2c\gamma^2}{16\pi(\boldsymbol{\mu}_{12}\cdot\mathbf{n}_E)^2}=\frac{\gamma^2}{2\omega_R^2}\,I\,, \tag{13.45}$$

allows us to write the cycle-averaged force in the form

$$\boxed{\langle\mathbf{F}\rangle \;=\; \frac{\hbar p}{1+p}\left[(\omega-\omega_o)\frac{\nabla E_o}{E_o}\;+\;\frac{\gamma}{2}\nabla\phi\right]}\;. \tag{13.46}$$

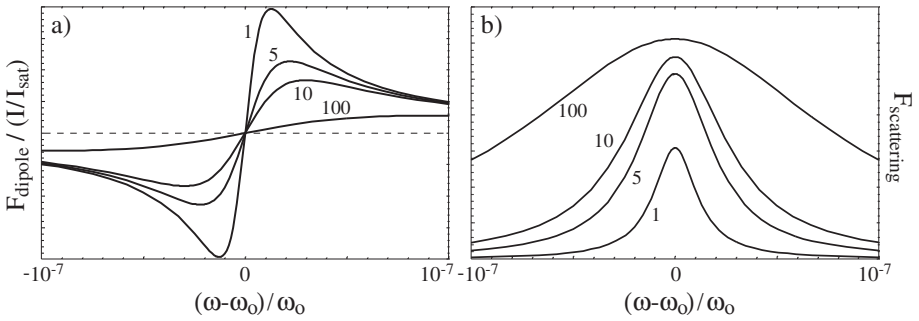

Figure 13.4: Dipole force and scattering force for sodium atoms ($1/\gamma=16.1ns$, $\lambda_o=590nm$) as a function of excitation frequency ω. The numbers in the figures indicate the value of the ratio I/I_{sat}.

This formula was originally developed by Gordon and Ashkin using a quantum mechanical derivation [8]. The present derivation uses quantum mechanics only for the calculation of the atomic polarizability (see Appendix **??**). It follows from quantum theory that the scattering force originates from cycles of absorption and spontaneous emission, whereas the dipole force is due to cycles of absorption and stimulated emission. Notice, that the maximum value for the saturation parameter p is obtained for exact resonance, i.e. $\omega = \omega_o$. In this case, the factor $p/(1+p)$ cannot exceed the value of one which limits the maximum value of the force (saturation). For an intensity of $I = I_{sat}$ ($I_{sat} \approx 1.6 mW$ for Rubidium atoms) the force amounts to one-half of the maximum force. For frequencies $\omega < \omega_o$ (red detuning) the dipole force is proportional to $-\nabla E_o$ causing an atom to be attracted towards regions of high intensity. On the other hand, for frequencies $\omega > \omega_o$ (blue detuning) atoms are repelled from regions of high intensity because the dipole force is proportional to ∇E_o. The dipole force vanishes for exact resonance. Fig. 13.4 shows the qualitatively the frequency behavior of the dipole and scattering force for different excitation intensities. Using $\mathbf{k} = \nabla\phi$ and conditions far from saturation, the scattering force can be written as

$$\langle \mathbf{F}_{scatt} \rangle \;=\; \hbar \mathbf{k} \, \frac{\gamma}{2} \, \frac{I}{I_{sat}} \, \frac{\gamma^2/4}{(\omega - \omega_o)^2 + \gamma^2/4} \quad I \ll I_{sat} \, . \tag{13.47}$$

which has a maximum for exact resonance. The influence of saturation on the scattering force is illustrated in Fig. 13.5.

In atom manipulation experiments the scattering force is used to cool atoms down to extremely low temperatures thereby bringing them almost to rest. At ambient conditions atoms and molecules move at speeds of about $1000\, m/s$ in random directions. Even at temperatures as low as $-270°C$ the speeds are on the order of

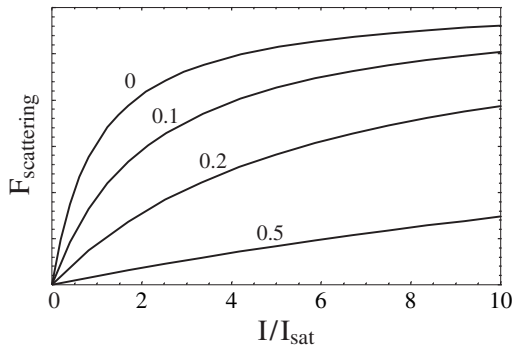

Figure 13.5: Scattering force for sodium atoms ($1/\gamma = 16.1 ns$, $\lambda_o = 590\, nm$) as a function of I/I_{sat}. The numbers in the figures indicate the frequency detuning in units of $10^7 (\omega - \omega_o)/\omega_o$.

$100\,m/s$. Only for temperatures close to absolute zero ($-273°C$) the motion of atoms slows down significantly. The initial idea to slow down the motion of atoms is based on the Doppler effect. It was first proposed by Hänsch and Schawlow in 1975 [5]. Neutral atoms are irradiated by pairs of counter propagating laser beams. If an atom moves against the propagation direction of one of the laser beams the frequency as seen from the atom will shift towards higher frequencies (blue shift) according to the Doppler effect. On the other hand, an atom moving in direction of beam propagation will experience a shift towards lower frequencies (red shift). If the laser frequency is tuned slightly below a resonance transition, an atom will predominantly absorb a photon when it moves against laser beam propagation [c.f. Eq. (13.47)]. The absorption process slows the atom down according to momentum conservation. Once the atom is excited it will eventually reemit its excitation energy by spontaneous emission which is a random process and does not favor any particular direction. Thus, averaged over many absorption/emission cycles, the atom moving towards the laser will lose velocity and effectively cool. To slow the atom down in all dimensions one requires six laser beams opposed in pairs and arranged in three directions at right angles to each other. Whichever direction the atom tries to move it will be met by photons of the right energy and pushed back into the area where the six laser beams intersect. The movement of the atoms in the intersection region is similar to the movement in a hypothetical viscous medium (optical molasses). It can be calculated that two-level atoms cannot by cooled below a certain temperature, called the Doppler limit [7]. For sodium atoms the limiting temperature is $240\mu K$ corresponding to speeds of $30\,cm/s$. However, it was experimentally found that much lower temperatures could be attained. After surpassing another limit, the so-called recoil limit which states that the speed of an atom should not be less than that imparted by a single photon recoil, temperatures as low as $0.18\,\mu K$ have been generated for helium atoms. Under these conditions the helium atoms move at speeds of only $2\,cm/s$. Once the atoms are sufficiently cold they would fall out of the optical molasses due to gravity. To prevent this from happening, an initial trapping scheme based on the dipole force allowed to grip the atoms at the focal point of a tightly focused beam [9]. Unfortunately, the optical dipole trap was not strong enough for most applications and a new three-dimensional trap based on the scattering force has been developed. This kind of trap is now called the magneto-optic trap. Its restoring force comes from a combination of oppositely directed circularly polarized laser beams and a weak, varying, inhomogeneous magnetic field with a minimum in the intersection region of the laser beams. The magnetic field strength increases with distance from the trap center and gives rise to a force towards the trap center.

13.3.4 Beyond the dipole approximation

In principle, any macroscopic object can be regarded to be composed of individual dipolar subunits. The self-consistent solution for the electric and magnetic fields generated by these dipoles is (see section **??**)

$$\begin{aligned} \underline{\mathbf{E}}(\mathbf{r}) &= \underline{\mathbf{E}}_o(\mathbf{r}) + \omega^2 \mu_o \sum_{n=1}^{N} \overleftrightarrow{\mathbf{G}}(\mathbf{r}, \mathbf{r}_n) \cdot \underline{\boldsymbol{\mu}}_n \\ \underline{\mathbf{H}}(\mathbf{r}) &= \underline{\mathbf{H}}_o(\mathbf{r}) - i\omega \sum_{n=1}^{N} \left[\nabla \times \overleftrightarrow{\mathbf{G}}(\mathbf{r}, \mathbf{r}_n)\right] \cdot \underline{\boldsymbol{\mu}}_n \qquad \mathbf{r} \neq \mathbf{r}_n \ , \end{aligned} \tag{13.48}$$

where we used the complex representation of the time-harmonic fields. $\overleftrightarrow{\mathbf{G}}$ denotes the dyadic Green's function, $\underline{\boldsymbol{\mu}}_n$ the electric dipole moment at $\mathbf{r} = \mathbf{r}_n$, and $\underline{\mathbf{E}}_o$, $\underline{\mathbf{H}}_o$ the exciting field. The system is assumed to consist of N individual dipoles. To first order, the dipole moment $\underline{\boldsymbol{\mu}}_n$ is

$$\underline{\boldsymbol{\mu}}_n = \alpha(\omega)\, \underline{\mathbf{E}}(\mathbf{r}_n) \ . \tag{13.49}$$

Combining equations 13.48 and 13.49 we obtain implicit equations for the fields $\underline{\mathbf{E}}$ and $\underline{\mathbf{H}}$ which can be solved by matrix inversion techniques. In principle, the mechanical force acting on an arbitrary object made of single dipolar subunits can be determined by using Eq. (13.38) in combination with Eqs. (13.48) and (13.49). However, if we require that the object does not deform under the influence of the electromagnetic field, the internal forces must cancel and the mechanical force is entirely determined

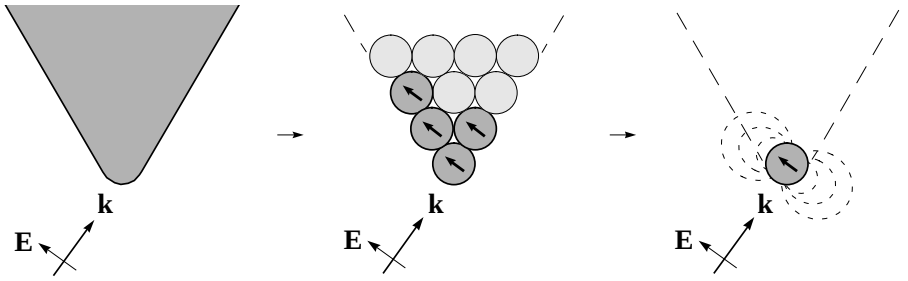

Figure 13.6: Illustration of the coupled dipole approach. A macroscopic object is subdivided into individual microscopic dipolar subunits. Each dipole moment can be calculated self-consistently by using the Green's function formalism. In a rough approximation the field in front of a metal tip can be replaced by the field of a single dipole. However, the parameters of the polarizability have to be deduced from a rigorous calculation.

by the fields outside of the object. In this case, the mechanical force can be determined by solving for the fields outside the object and evaluating Maxwell's stress tensor according to Eqs. (13.10) and (13.15).

13.4 Optical tweezers

In 1986 Ashkin and co-workers showed that a single tightly focused laser beam could be used to hold, in three dimensions, a microscopic particle near the beam focus. This has now become established as a powerful noninvasive technique and is known as *optical tweezers* [2]. Optical tweezers have found widespread application especially in biology and have been used to manipulate dielectric spheres, living cells, DNA, bacteria, and metallic particles. Optical tweezers are routinely applied to measure elasticity, force, torsion and position of a trapped object. Forces measured with optical tweezers are typically in the $1-10pN$ range. While trapping of small particles (diameters $d \ll \lambda$) is well explained by the dipole force [first term in Eq. (13.38)], a theory for trapping of larger particles requires an extension of the dipole approximation by including higher multipole orders, similar to Mie scattering. The trapping force can be represented in the form

$$\left\langle \mathbf{F}(\mathbf{r}) \right\rangle = \mathbf{Q}(\mathbf{r}) \, \frac{\varepsilon_s^2 \, P}{c} \, , \tag{13.50}$$

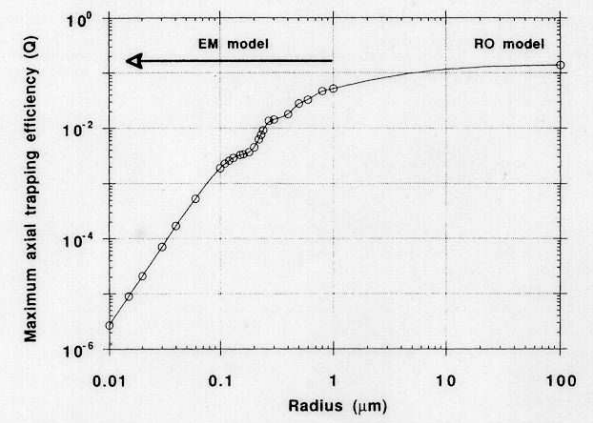

Figure 13.7: Calculated maximum axial trapping efficiency $Max[Q_z(x=0, y=0, z)]$ for a polystyrene particle ($\varepsilon = 2.46$) with variable radius r_o irradiated by a focused Gaussian beam. The surrounding medium is water ($\varepsilon_s = 1.77$) and the numerical aperture is $NA = 1.15$. From Ref. [10].

where ε_s is the dielectric constant of the surrounding medium, P is the power of the trapping beam, and c is the vacuum speed of light. The dimensionless vector $\mathbf{Q}$ is called the trapping efficiency. In the dipole limit and in absence of particle losses, $\mathbf{Q}$ depends on the normalized gradient of the light intensity and the polarizability α given by

$$\alpha(\omega) \;=\; 3\varepsilon_o V_o \frac{\varepsilon(\omega)-\varepsilon_s(\omega)}{\varepsilon(\omega)+2\varepsilon_s(\omega)}\;, \tag{13.51}$$

where V_o and ε are the particle's volume and dielectric constant, respectively. Fig. 13.7 shows the maximum axial trapping efficiency $Max[Q_z(x=0,y=0,z)]$ for a polystyrene particle ($\varepsilon=2.46$) with variable radius r_o irradiated by a focused Gaussian beam. For small particles ($r_o<100nm$) the trapping efficiency scales as r_o^3 in accordance with the dipole approximation and Eq. (13.51). However, for larger particles, the dipole approximation becomes inaccurate.

As illustrated in Fig. 13.8, a simple ray optical analysis can be applied to describe trapping of particles larger than the wavelength. In this model, every refraction of a light ray at the particle surface transfers momentum from the trapping laser to the particle. The time rate of change of the momentum is the trapping force. The total force can be calculated by representing the light beam as a collection of rays (see section **??**), and summing the forces due to each of the rays. Stable trapping requires that there is a position for which the net force on the particle is zero and any displacement

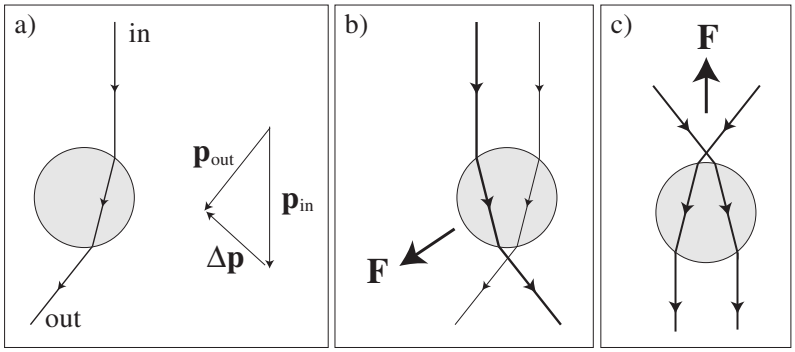

Figure 13.8: Illustration of the ray-optic picture for optical trapping of particles larger than the wavelength. a) A single ray is refracted twice at the surface of the particle. The net momentum change $\Delta\mathbf{p}$ is calculated by the vectorial difference of the momenta of incoming and outgoing rays. Momentum conservation requires that the momentum transfered to the particle is $-\Delta\mathbf{p}$. b) Refraction of two light rays with different intensites. The particle is pulled towards the higher intensity. c) Axial trapping of a particle in a single beam trap. A particle initially located beneath the focus is pulled towards the focus.

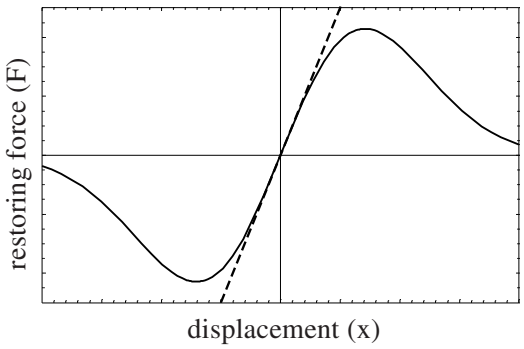

Figure 13.9: Linear approximation (dashed line) to the restoring force (solid line) for a single beam gradient trap. The slope of the linear approximation is denoted as trap stiffness k. It depends on the particle polarizability, laser power, and field gradients.

results in a restoring force towards the 'zero-force' position. The reader is refered to the work of Ashkin for further details on optical trapping in the ray optics regime [11].

An important concept in applications of laser tweezers is the trap *stiffness* k. For small displacements x from the equilibrium position, the trapping potential can be approximated by a harmonic function and the restoring force becomes linearly dependent on x

$$\langle F \rangle \;=\; k\,x\;. \tag{13.52}$$

In principle, k is a tensor of rank two since the stiffness depends on the direction of displacement. For a single beam gradient trap it is often sufficient to distinguish between transverse and longitudinal stiffness. The trap stiffness depends on the particle's polarizability, the excitation power and the field gradients. Fig. 13.9 illustrates the linear approximation for a paraxial Gaussian beam. The trap stiffness can be measured experimentally by using the viscous drag force F_d acting on a particle inside a madium with relative velocity v. For a spherical particle with radius r_o, F_d is described by Stokes' law

$$\langle F_d \rangle \;=\; 6\pi\,\eta\,r_o\,v\;. \tag{13.53}$$

Here, η is the viscosity of the medium ($10^{-3} Ns/m^2$ for water) and it is assumed that inertial forces are negligible (small Reynolds number). Thus, by moving the surrounding medium with velocity v past a stationary trapped particle of known size, Stoke's law determines the force $\langle F_d \rangle$ exerted on the particle. This force has to be balanced by the trapping force $\langle F \rangle$ in Eq. (13.52) which allows us to determine the stiffness k by measuring the displacement x. There are different ways to establish a relative speed v between particle and surrounding medium: 1) the medium is pumped past a stationary particle using a flow chamber, 2) the chamber containing the medium is

moved past a stationary particle using piezo-transducers or a motorized stage, and 3) the optical trap is moved using beam-steering methods while the medium remains stationary. No matter what the method is, the calibration of k relies on an accurate measurement of the displacement x. Most commonly, x is determined by refocusing the scattered light from the trapped particle onto a position sensitive detector, such as a silicon quadrant detector [12].

Brownian motion has to be taken into account if the depth of the trapping potential is not negligible compared with the energy kT. In fact, stable trapping requires often a trap depth of $\approx 10kT$. Brownian motion leads to noise in force measurements giving rise to a characteristic power spectrum [3]. Unfortunately, the Langevin equation cannot be solved for a trapping potential with finite depth. Therefore, to answer questions regarding trap stability it is necessary to solve the Fokker-Planck equation [13].

13.5 Angular Momentum and Torque

Besides energy and momentum, an electromagnetic field can also carry angular momentum which exerts a mechanical torque on an irradiated structure. This torque can be calculated from a conservation law for angular momentum similar to Eq. (13.13)

$$-\int_{\partial V}\left[\overleftrightarrow{\mathbf{T}}\,(\mathbf{r},t)\times\mathbf{r}\right]\cdot\mathbf{n}(\mathbf{r})\,da \;=\; \frac{d}{dt}\left[\mathbf{J}_{field}+\mathbf{J}_{mech}\right]. \tag{13.54}$$

As before, ∂V denotes the surface of a volume enclosing the irradiated structure, $\mathbf{n}$ is the unit vector perpendicular to the surface, and da is an infinitesimal surface element. $\mathbf{J}_{field}$ and $\mathbf{J}_{mech}$ denote the total mechanical and electromagnetic angular momentum, respectively, and $[\overleftrightarrow{\mathbf{T}}\times\mathbf{r}]$ is the angular-momentum flux-density pseudotensor. The mechanical torque $\mathbf{N}$ acting on the irradiated structure is defined as

$$\mathbf{N}=\frac{d}{dt}\mathbf{J}_{mech}\,. \tag{13.55}$$

For a monochromatic field the time-averaged torque can be represented as

$$\boxed{\langle\mathbf{N}\rangle \;=\; -\int_{\partial V}\left\langle\overleftrightarrow{\mathbf{T}}\,(\mathbf{r},t)\times\mathbf{r}\right\rangle\cdot\mathbf{n}(\mathbf{r})\;da}\,, \tag{13.56}$$

where we have used the fact that $\langle d\mathbf{J}_{field}/dt\rangle = 0$. Equation (13.56) allows us to calculate the mechanical torque acting on an arbitrary body within the closed surface ∂V. The torque is entirely determined by the electric and magnetic fields on the surface ∂V.

One of the first demonstrations of angular momentum transfer from an optical beam to an irradiated object was performed by Beth in 1936 [14]. He measured the torque on a suspended birefringent half-wave plate as circularly polarized light passed through it. This experiment provided evidence that the angular momentum per photon in a pure circularly polarized state is $\hbar$. Since Beth's experiment, various demonstrations have been performed demonstrating that optical beams with non-vanishing angular field momentum can indeed be used to promote a trapped particle into a spinning state [15] and applications as optical and biological micromachines have been suggested [16].

13.6 Forces in optical near-fields

Optical near-fields are mainly composed of evanescent field terms which decay rapidly with distance from the source. This fast decay leads to strong field gradients and thus to strong dipole forces. Evanecent waves created by total internal reflection at a glass-air interface have been used as atomic mirrors. In these experiments, an atomic beam incident on the interface is deflected by the dipole force exerted by the evanescent field if the light frequency is tuned to the blue side of an electronic resonance [18]. Evanescent fields have also been used to accelerate micrometer sized particles along a plane surface and along planar waveguides by means of the scattering force [19]. Optical near-field traps have been proposed for atom trapping [17] and also for the manipulation of polarizable particles with diameters down to $10nm$ [24]. The strongest dipole forces arise from strongly enhanced fields near material edges, corners, gaps, and tips. Therefore, as an application of the theory developed in Section 13.3 we calculate the forces near a sharp metal tip.

The electric field distribution for a laser illuminated gold tip is strongly polarization dependent [24]. Fig. 13.10 shows the electric field distribution (calculated with the MMP method) near a sharply pointed gold tip irradiated with a monochromatic plane wave polarized along the tip axis. The field lines are slightly distorted by a small particle in the vicinity of the tip. The arrow indicates the trapping force acting on the particle. While the intensity at the foremost part of the tip is strongly enhanced over the intensity of the excitation light, no enhancement beneath the tip is observed when the exciting light is polarized perpendicular to the tip axis. Calculations for platinum and tungsten tips show lower enhancements, whereas the field beneath a glass tip is reduced compared to the excitation field.

The enhanced field at the tip results from an increase of surface charge density. The incident light drives the free electrons in the metal along the direction of polarization. While the charge density is zero inside the metal at any instant of time

($\nabla \cdot \mathbf{E} = 0$), charges accumulate on the surface of the metal. When the incident polarization is perpendicular to the tip axis, diametrically opposed points on the tip surface have opposite charges. As a consequence, the foremost end of the tip remains uncharged. On the other hand, when the incident polarization is parallel to the tip axis (c.f. Fig. 13.10), the induced surface charge density is rotationally symmetric and has the highest amplitude at the end of the tip. In both cases the surface charges form a standing wave oscillating with the frequency of the excitation light but with wavelengths shorter than the wavelength of the exciting light (surface plasmons).

With the field distribution around the tip determined the force acting on the particle can be calculated by evaluating Maxwell's stress tensor. However, in order to avoid elaborate computations, we represent both tip and particle by point dipoles. The dipole force acting on a Rayleigh particle can be easily calculated as [c.f. Eq. (13.41)]

$$\langle \mathbf{F} \rangle = (\alpha'/2)\, \nabla \langle |\mathbf{E}|^2 \rangle = (\alpha'/2)\, \nabla (\underline{\mathbf{E}} \cdot \underline{\mathbf{E}}^*) \,, \tag{13.57}$$

where α' is the real part of the polarizability of the particle and $\mathbf{E}$ is the electric field

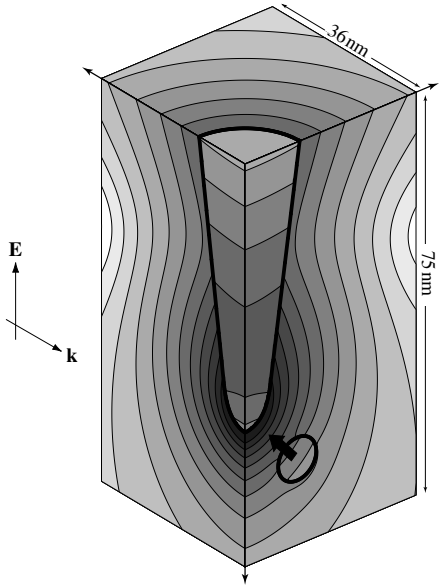

Figure 13.10: Trapping of a dielectric particle by a laser-irradiated gold tip in water. The figure shows contourlines of $E^2 = \underline{\mathbf{E}} \cdot \underline{\mathbf{E}}^*$ (factor of 2 between successive lines) for plane wave excitation with $\lambda = 810nm$ and polarization along the tip axis. The dielectric constants of tip, particle and water at $\lambda = 810nm$ are $\varepsilon = -24.9 + 1.57i$, $\varepsilon = 2.5$ and $\varepsilon = 1.77$, respectively. The diameters of tip and particle are $10nm$. The arrow indicates the direction of the trapping force.

in the absence of the particle. The particle tends to move to the higher intensity region where its induced dipole has lower potential energy. We neglect the scattering force [second term in Eq. (13.41)] because of the small particle size and because there is no radiation pressure associated with the near-fields. The assumptions inherent in Eq. (13.57) are that the external field is homogeneous across the particle and that the particle does not alter the field $\mathbf{E}$ in Eq. (13.57). These assumptions, however, do not hold for a the particle shown in Fig. 13.10. The intensity contours are distorted around the particle and the field inside is highly inhomogeneous. Nevertheless, it will be shown later by comparison with the exact solutions of Ref. [24] that the point-dipole approximation leads to errors which are less than one order of magnitude.

The situation to be analyzed is shown in Fig. 13.11. The metal tip is illuminated by a plane wave at right angle such that the polarization is parallel to the tip axis. The factor f of the enhanced electric field intensity in front of the tip is determined by the material properties, the sharpness and shape of the tip, and the wavelength of the illuminating field [21-23]. We denote the dipoles of tip and particle by $\boldsymbol{\mu}_t$ and $\boldsymbol{\mu}$, respectively. Without loss of generality, the tip dipole is placed at the origin of the coordinate system. To further simplify the situation, we assume that the coupling between tip and particle can be neglected. In this limit, the incident field $\mathbf{E}_o$ excites a dipole moment $\boldsymbol{\mu}_t$ in the tip and the fields generated by $\boldsymbol{\mu}_t$ induce a dipole moment $\boldsymbol{\mu}$ in the particle.

According to the coupled dipole formalism, any object can be subdivided into

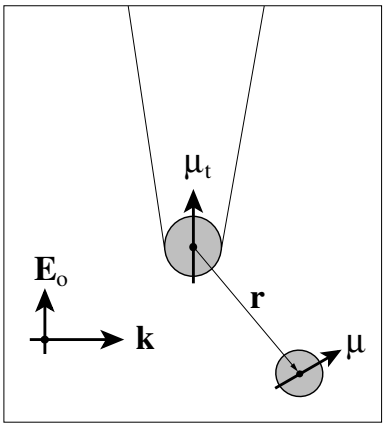

Figure 13.11: Trapping of a particle by a laser illuminated metal tip. The tip is illuminated by a plane wave polarized along the tip axis. Both tip and particle are represented by dipoles.

dipolar subunits. In a metal, these units have to be chosen so dense that the field at the tip cannot be attributed to the closest dipole alone. Consequently, the metal tip cannot be approximated by a single polarizable sphere as it is often done for dielectric tips [25]. However, as shown in Fig. 13.12, rigorous calculations show that the spatial distribution of the fields close to the metal tip are similar to the field of a vertical dipole. The dipole moment $\boldsymbol{\mu}_t$ can be expressed in terms of the computationally determined enhancement factor, f, for the electric field intensity as

$$\mathbf{E}(x=0, y=0, z=r_t) \;=\; \frac{2\;\boldsymbol{\mu}_t}{4\pi\varepsilon_o\varepsilon_s\, r_t^3} \;\equiv\; \sqrt{f}\,\mathbf{E}_o\;, \tag{13.58}$$

where r_t denotes the tip radius ($z=r_t$ is the foremost end of the tip) and ε_s is the dielectric constant of the environment. Eq. (13.58) allows us to calculate the dipole moment of the tip as a function of tip size and enhancement factor. Since we consider tip-particle distances d for which $kd \ll 1$ we only retain the dipole's near-field from which we calculate

$$\underline{\mathbf{E}} \cdot \underline{\mathbf{E}}^* \;=\; \frac{|\boldsymbol{\mu}_t|^2}{(4\pi\varepsilon_o\varepsilon_s)^2}\;\frac{1\;+\;3(z/r)^2}{r^6}\;, \tag{13.59}$$

where $r = |x^2+y^2+z^2|$. A comparison between the non-retarded fields of a single dipole and the computationally determined fields for the laser illuminated metal tip is shown in Fig. 13.12.

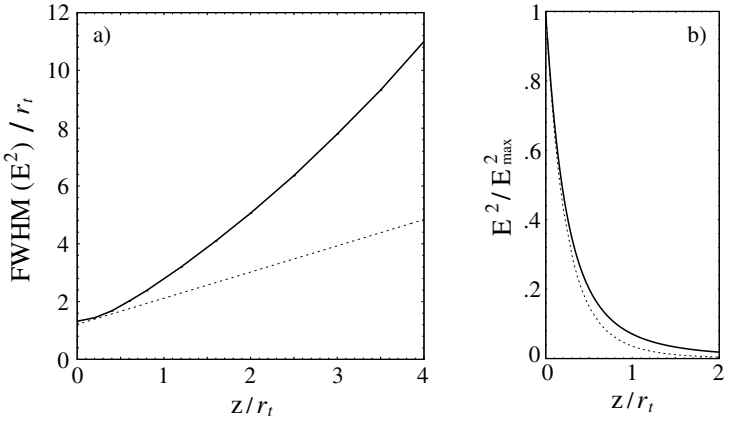

Figure 13.12: Comparison of the nonretarded fields of a single dipole (dotted curves) and the computationally determined fields for a laser illuminated metal tip (solid curves). Figure a) shows the lateral spread of the field (perpendicular to tip axis) as a function of the distance z from the foremost point of the tip. Figure b) shows the decay of the field along the tip axis. All distances are normalized with the tip radius $r_t = 5nm$.

Using Eq. (13.59) together with the expression for $\alpha(\omega)$ in Eq. (13.51), the force acting on the polarizable particle located at (x, y, z) is determined by Eq. (13.57) as

$$\langle \mathbf{F} \rangle \;=\; -\frac{3\, r_t^6\, f\, E_o^2\, \alpha'}{4\, r^6} \left[\rho\, (1 + 4\, z^2/r^2) \mathbf{n}_\rho \;+\; 4\, z^3/r^2 \mathbf{n}_z \right] \;. \tag{13.60}$$

Here, $\mathbf{n}_z$ and $\mathbf{n}_\rho$ denote the unit vectors along the tip axis and in transverse direction, respectively, and the transverse distance is $\rho = x^2 + y^2$. The minus sign indicates that the force is directed towards the tip. We find that $\langle \mathbf{F} \rangle$ is proportional to the enhancement factor f, the intensity of the illuminating light $I_o = 1/2 \sqrt{\varepsilon_o \varepsilon_s / \mu_o}\, E_o^2$, the real part of the particle polarizability α', and the sixth power of the tip radius a_t. It has to be kept in mind, that f and r_t are not independent parameters; their relationship can be determined by rigorous calculations only.

We now calculate the potential energy of the particle in the field of the tip dipole (trapping potential) as

$$V_{pot}(\mathbf{r}) \;=\; -\int_\infty^{\mathbf{r}} \langle \mathbf{F}(\mathbf{r}') \rangle \, d\mathbf{r}' \;. \tag{13.61}$$

The integration path from $\mathbf{r}$ to ∞ is arbitrary because $\mathbf{F}$ is a conservative vector field. After carrying out the integration we find

$$V_{pot}(\mathbf{r}) \;=\; -r_t^6\, f\, E_o^2\, \alpha'\, \frac{1 + 3\, z^2/r^2}{8 r^6} \;. \tag{13.62}$$

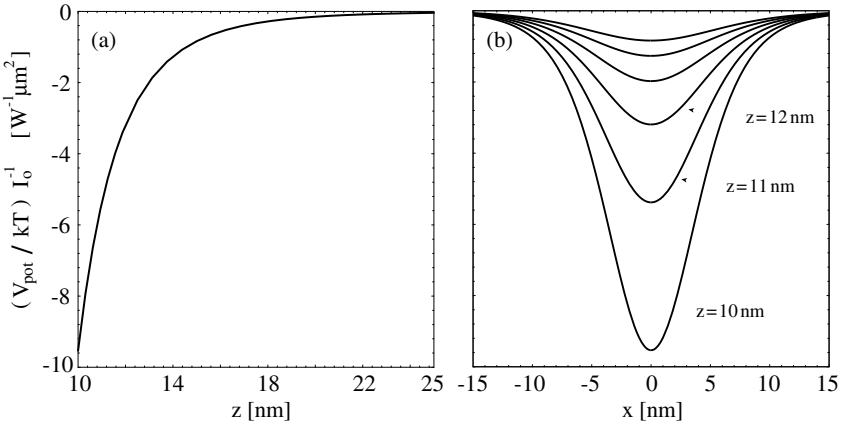

Figure 13.13: Trapping potential V_{pot} along the tip axis (a) and along a transverse direction at $z = r_t + r_o$ beneath the tip. An enhancement factor of $f = 3000$ is assumed. The radii of tip and particle are $r_t = r_o = 5nm$. The dielectric constants of particle and environment are $\varepsilon = 2.5$ and $\varepsilon_s = 1.77$ (water), respectively. The forces are normalized with $k_B T$ and the incident intensity I_o.

The maximum value of V_{pot} is reached exactly in front of the tip $z = r_o + r_t$, r_o being the particle's radius. Fig. 13.13 shows V_{pot} along the tip axis and along a transverse axis immediately in front of the tip. Since in aqueous environments the trapping forces compete with Brownian motion, the potential in is normalized with $k_B T$ (k_B = Boltzmann constant, $T = 300\,K$). Additionally, the curves are scaled with the incident intensity I_o. To have a trapping potential which is just equal to $k_B T$ at room temperature, an intensity of $I_o \approx 100 mW/\mu m^2$ is required.

Let us assume for the following that a sufficient condition for trapping is $V_{pot} > k_B T$. We can then calculate the intensity required to trap a particle of a given size. Using the expression for the particle polarizability and evaluating Eq. (13.62) at $\mathbf{r} = (r_t + r_o)\mathbf{n}_z$ we find

$$I_o \;>\; \frac{kTc}{4\pi\sqrt{\varepsilon_s}}\,\mathrm{Re}\left\{\frac{\varepsilon + 2\,\varepsilon_s}{\varepsilon_p - \varepsilon_s}\right\}\,\frac{(r_t + r_o)^6}{f\,r_t^6\,r_o^3}\;. \tag{13.63}$$

The curve for which the equality holds is shown in Fig. 13.14. The minimum in the curve indicates that the incident intensity and the tip radius can be adjusted to selectively trap particles with sizes in a limited range. Too small particles are not trapped because their polarizability is too small. On the other hand, for too big particles the minimum separation between tip and particle $(r_t + r_o)$ becomes too large. For the presently used parameters the optimum particle size is $r_o \approx 5nm$. However, since the trapping fields decay slower the larger the tip radius is, it can be expected that for larger tip sizes the optimum particle size becomes larger. As a rule of thumb, the particle size should be in the range of the tip size.

Notice, that instead of calculating first the trapping force, the potential $V_{pot}(\mathbf{r})$

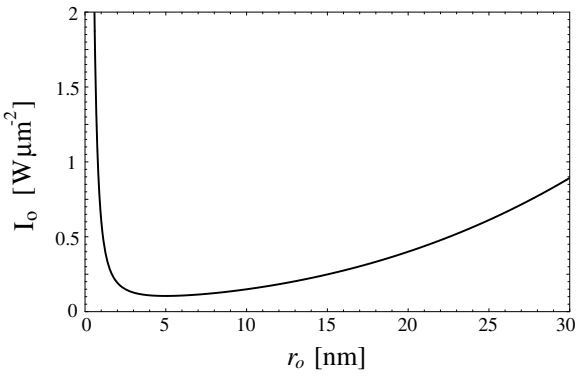

Figure 13.14: Minimum trapping intensity I_o as a function of the particle radius r_o. An enhancement factor of $f = 3000$ is assumed and the tip radius is $r_t = 5nm$.

could have been easier determined by considering the interaction energy of the particle in the dipole approximation. With $\mathbf{E}$ being the field of the tip dipole $\boldsymbol{\mu}_t$ it is easy to show that

$$V_{pot}(\mathbf{r}) \;=\; -\boldsymbol{\mu}\cdot\mathbf{E}(\mathbf{r}) \;=\; -(\alpha'/2)\,E^2(\mathbf{r})\;, \tag{13.64}$$

leads to the same result as Eq. (13.62).

The simple two-dipole model applied here renders a trapping potential whose general shape is in very good agreement with the results in Ref. [24]. A comparison shows that the here calculated forces are off by a factor $\approx 2-3$. Nevertheless, we find that moderate laser powers are needed to trap a nanoparticle at the end of a gold tip in an aqueous environment. Experiments have shown that the formation of eddy currents in the aqueous environment does have an effect on the trapping scheme. These eddy currents are generated by laser heating of the metal tip.

Problems

Problem 13.1 A spherical glass particle in water is trapped at the focus of a monochromatic paraxial Gaussian beam with $\lambda = 800nm$ and variable NA (see section **??**). The polarizability of the particle is

$$\alpha \;=\; 3\varepsilon_o V_o \frac{\varepsilon - \varepsilon_w}{\varepsilon + 2\varepsilon_w} \;, \tag{13.65}$$

where V_o is the volume of the particle, and the dielectric constants of glass and water are $\varepsilon = 2.25$ and $\varepsilon_w = 1.76$, respectively.

1. Show that for small transverse displacements (x) from the focus the force is proportional to x. Determine the spring constant as a function of NA, d_o, λ, and P_o, where d_o is the particle diameter and P_o the laser power.
2. Is it possible to derive in the same way a spring constant for longitudinal displacements z? If yes, calculate the corresponding spring constant as a function of NA, d_o, and P_o.
3. Assume $NA = 1.2$ and $d_o = 100nm$. What intensity is necessary in order to create a trapping potential $V > 10kT$, where k is Boltzmann's constant and $T = 300K$ is the ambient temperature? What is the restoring force for a transverse displacement of $x = 100nm$?

Problem 13.2 Consider the total internal reflection of a plane wave with wavelength $\lambda = 800nm$ incident at an angle $\theta = 70°$ from the normal of a glass-air interface ($\varepsilon = 2.25$). The plane wave is incident from the glass-side and is s-polarized. The normal of the interface is parallel to the gravitational axis and the air-side is pointing to the bottom. A tiny glass particle is trapped on the air-side in the evanescent field generated by the totally internally reflected plane wave. Calculate the minimum required intensity I of the plane wave to prevent the glass particle from falling down [α given by Eq. (13.65) with $\varepsilon_w = 1$]. The specific density of glass is $\rho = 2.2\,10^3 kg/m^3$ and the particle diameter is $d_o = 100nm$. What happens if the particle size is increased?

Problem 13.3 A particle is placed into the field of two counter propagating plane waves of identical amplitudes, phases and polarizations. The particle is trapped inside a transverse sheet formed by the constructive interference of the two waves. The intensity of one single plane wave is I and the polarizability of the particle is α. Calculate the required energy to promote the particle from one lobe to the next a function of I.

Problem 13.4 Calculate the mutual attraction force between two identical dipolar particles which are irradiated by a plane wave polarized along the axis defined by the two particle centers. Plot the force as a function of particle distance and use suitable normalizations for the axes.

Problem 13.5 Evaluate Maxwell's stress tensor on a spherical surface enclosing a Rayleigh particle irradiated by a plane wave. What does the result tell you?

References

[1] R. Frisch, "Experimenteller Nachweis des Einsteinischen Strahlungsrückstosses," *Z. Phys.* **86**, 42–45 (1933).

[2] A. Ashkin, "Optical trapping and manipulation of neutral particles using lasers," *Proc. Natl. Acad. Sci. USA* **94**, 4853–4860 (1987).

[3] K. Svoboda and S. T. Block, "Biological applications of optical forces," *Annu. Rev. Biophys. Biomol. Struct.* **23**, 247–285 (1994).

[4] B. Pringsheim, "Zwei Bemerkungen über den Unterschied von Lumineszenz-und Temperaturstrahlung," *Z. Phys.* **57**, 739–741 (1929).

[5] T. W. Hänsch and A. L. Schawlow, "Cooling of gases by laser radiation," *Opt. Commun.* **13**, 68–69 (1975).

[6] Y. Shimizu and H. Sasada, "Mechanical force in laser cooling and trapping," *Am. J. Phys.* **66**, 960–967 (1998).

[7] S. Stenholm, "The semiclassical theory of laser cooling," *Rev. Mod. Phys.* **58**, 699–739 (1986).

[8] J. P. Gordon and A. Ashkin, "Motions of atoms in a radiation trap," *Phys. Rev. A* **21**, 1606–1617 (1980).

[9] S. Chu, J. E. Bjorkholm, A. Ashkin, and A. Cable, "Experimental observation of optically trapped atoms," *Phys. Rev. Lett.* **57**, 314–317 (1986).

[10] W. H. Wright, G. J. Sonek, and M. W. Berns, "Radiation trapping forces on microspheres with optical tweezers," *Appl. Phys. Lett.* **63**, 515–517 (1993).

[11] A. Ashkin, "Forces of a single-beam gradient laser trap on a dielectric sphere in the ray optics regime," *Biophys. J.* **61**, 569–582 (1992).

[12] F. Gittes and C. F.Schmidt, "Interference model for back-focal-plane displacement detection in optics tweezers," *Opt. Lett.* **23**, 7–9 (1998).

[13] R. Zwanzig, "Nonequilibrium Statistical Mechanics," Oxford University Press (2001).

[14] R. A. Beth, "Mechanical detection and measurement of the angular momentum of light," *Phys. Rev.* **50**, 115–125 (1936).

[15] See, for example, T. A. Nieminen, N. R. Heckenberg, and H. Rubinsztein-Dunlop, "Optical measurement of microscopic torques," *J. Mod. Opt.* **48**, 405–413 (2001).

[16] See, for example, L. Paterson, M. P. MacDonald, J. Arlt, W. Sibbett, P. E. Bryant, and K. Dholakia, "Controlled rotation of optically trapped microscopic particles," *Science* **292**, 912–914 (2001).

[17] S. K. Sekatskii, B. Riedo and G. Dietler, "Combined evanescent light electrostatic atom trap of subwavelength size," *Opt. Comm.* **195**, 197–204 (2001).

[18] For a review, see, C. S. Adams, M. Sigel, and J. Mlynek, "Atom optics," *Phys. Rep.* **240**, 143–210 (1994).

[19] S. Kawata and T. Tani, "Optically driven Mie particles in an evanescent field along a channeled waveguide," *Opt. Lett.* **21**, 1768–1770 (1996).

[20] L. Novotny, "Allowed and forbidden light in near-field optics. II. Interacting dipolar particles," *J. Opt. Soc. Am. A* **14**, 105–113 (1997).

[21] L. Novotny, E. J. Sanchez, and X. S. Xie, "Near-field optical imaging using metal tips illuminated by higher-order Hermite-Gaussian beams," *Ultramicroscopy* **71**, 21–29 (1998).

[22] O. J. F. Martin and C. Girard, "Controlling and tuning strong optical field gradients at a local probe microscope tip apex," *Appl. Phys. Lett.* **70**, 705–707 (1997).

[23] W. Denk and D. W. Pohl, "Near-field optics: Microscopy with nanometer-size fields," *J. Vac. Sci. and Technol. B* **9**, 510–513 (1991).

[24] L. Novotny, R. X. Bian, and X. S. Xie, "Theory of nanometric optical tweezers," *Phys. Rev. Lett.* **79**, 645–648 (1997).

[25] D. V. Labeke and D. Barchiesi, "Theoretical problems in scanning near-field optical microscopy," in *Near Field Optics* (D. W. Pohl and D. Courjon, eds.) **242** of *NATO Advanced Study Institute, Series E*, 157–178, Dordrecht: Kluwer Academic Publishers (1993).